https://doi.org/10.2352/ISSN.2470-1173.2017.5.SD&A-368

Pixel-Based Adaptive Normalized Cross Correlation for Illumination Invariant Stereo Matching

Yong-Jun Chang, Yo-Sung Ho
Gwangju Institute of Science and Technology (GIST)
123 Cheomdangwagi-ro, Buk-gu, Gwangju, 61005, South Korea
Email: {yjchang, hoyo}@gist.ac.kr

Abstract

Stereo matching methods estimate a disparity value of the object as depth information. In general, most stereo matching methods are tested under ideal radiometric conditions. However, those ideal conditions cannot exist in real life. Adaptive normalized cross correlation (ANCC) is a method that is robust to radiometric variation. It estimates significantly accurate disparity values in the illumination variant condition. However, it has a high complexity problem in the cost computation because of the block matching-based method and the bilateral filtering process. In this paper, we propose a pixel-based ANCC using hue and gradient information to improve the computation complexity problem. The results show that the cost computation time is reduced even though error rates corresponding to the exposure and illumination changes have larger variations than those of the ANCC result.

Keywords: Stereo matching, disparity map, global mean value, hue transform

1. Introduction

In recent years, as interest in three-dimensional (3D) images has increased, various 3D contents have been created for applications such as stereoscopic display, super multi-view display, virtual reality (VR), and augmented reality (AR). Most 3D content utilize captured scenes and objects with their depth values for generating realistic content. There are several ways to acquire the depth value from the object or the captured scene. The depth camera uses two different types for the depth estimation: the time-of-flight (ToF) and the structured light. The depth camera measures the depth value of the object quickly and easily; however, measurement of depth value is affected by sunlight. The measurement distance of the depth camera is also limited because of the hardware problem. Therefore, passive sensor-based methods are also used.

One famous passive method is stereo matching. Two-dimensional (2D) stereo images are used for the stereo matching. Each image has a different viewpoint. For the depth estimation using stereo matching methods, correspondences between two images are searched first. Next, a disparity value between two corresponding points is calculated. The disparity value represents depth information of those corresponding points. In this way, disparity maps that represent depth information of captured stereo images are created.

In the stereo matching method, searching correspondences has an influence on the accuracy of the disparity map. Therefore, it is important to find exact correspondences. Moreover, the stereo matching method is usually performed assuming that the image rectification is used; therefore, correspondences are searched in the same scan line [1]. To calculate the similarity between two pixels, various similarity measures are used. There are generally two approaches for the similarity measure: a pixel-based and a patch-based measure. The pixel-based measure calculates the matching cost faster than the patch-based measure. However, the pixel-based measure usually has a matching ambiguity problem. For this reason, the patch-based measure is generally used for the similarity measure.

One of the approaches to improve the accuracy of the disparity search is a cross-scale cost aggregation [2]. It aggregates matching costs using disparity volumes and the filter kernel [3]. This cost aggregation method considers matching cost comparison not only to neighboring pixels but also to pixels of other scales. Using this cost aggregation method, relatively accurate disparity values can be searched even if the similarity measure is performed on a pixel basis. Another approach for the enhancement of the disparity search is a global stereo matching method. This method uses an energy function to measure the similarity between the current pixel and the correspondence pixel. The energy function is composed of the data term and the smoothness term. Since the global method considers the neighboring pixel's disparity values for the determining the current pixel's disparity value, it generates significant accurate disparity maps.

In general, it is assumed that many stereo matching methods are performed under ideal lighting conditions. However, it is difficult to obtain ideal lighting conditions for the actual stereo matching process. To perform illumination invariant stereo matching, several stereo matching methods are proposed such as an adaptive normalized cross correlation (ANCC) and a fast cost computation method using binary information [4-6]. In this paper, we propose a pixel-based ANCC, which is a fast and robust method, to mitigate the issues arising from radiometric variation.

2. Adaptive Normalized Cross Correlation

2.1 Color Image Formation Model

The adaptive normalized cross correlation (ANCC) calculates the matching cost independently from the lighting change factors [4]. For the cost computation that is independent from the lighting factors, the ANCC uses a color image formation model [7].

$$\begin{pmatrix} R_L(p) \\ G_L(p) \\ B_L(p) \end{pmatrix} \rightarrow \begin{pmatrix} \widetilde{R_L}(p) \\ \widetilde{G_L}(p) \\ \widetilde{B_L}(p) \end{pmatrix} = \begin{pmatrix} \rho_L(p) a_L R_L^{\gamma_L}(p) \\ \rho_L(p) b_L G_L^{\gamma_L}(p) \\ \rho_L(p) c_L B_L^{\gamma_L}(p) \end{pmatrix} \quad (1)$$

The color formation model shows how color values are stored on the device. It is defined in Eq. 1. Where R_L, G_L, and B_L are raw

colors of the current pixel p in the left viewpoint image. In Eq. 1, raw colors are stored as non-linear forms such as $\widetilde{R_L}$, $\widetilde{G_L}$, and $\widetilde{B_L}$. Those non-linear color values include three kinds of lighting factors: a brightness factor, a scale factor, and a gamma exponent. ρ_L and γ_L represent the brightness factor and the gamma exponent, respectively. Those two factors are applied to the three-color channels as the same value. Conversely, the scale factor is represented by different values such as a_L, b_L, and c_L, depending on the color channel type.

2.2 Elimination of Lighting Factors

The ANCC method removes lighting factors to perform the illumination invariant stereo matching. Non-linear color values in Eq. 1 are transformed to logarithmic values to eliminate the brightness factor ρ_L as shown in Eq. 2.

$$R'_L(p) = \log\rho_L(p) + \log a_L + \gamma_L \log R_L(p) \tag{2}$$

In Eq. 2, R'_L implies the logarithmic value of $\widetilde{R_L}$. The remaining $\widetilde{G_L}$ and $\widetilde{B_L}$ are converted to logarithmic values G'_L and B'_L in a similar manner. Subsequently, the average of logarithmic values of the three color channels is calculated as follows

$$I'_L(p) = \frac{R'_L(p) + G'_L(p) + B'_L(p)}{3} \tag{3}$$

where I'_L indicates the average value of three logarithmic color values. In order to remove the brightness factor, I'_L is subtracted from R'_L. Eq. 4 illustrates the removal of the brightness factor.

$$R''_L(p) = R'_L(p) - \frac{R'_L(p) + G'_L(p) + B'_L(p)}{3} \tag{4}$$

In Eq. 4, R''_L is the value with the brightness factor removed from R channel. Eq. 4 is redefined as follows

$$R''_L(p) = \log\frac{a_L}{\sqrt[3]{a_L b_L c_L}} + \gamma_L \log\frac{R_L(p)}{\sqrt[3]{R_L(p)G_L(p)B_L(p)}} \tag{5}$$

where $\log\frac{a_L}{\sqrt[3]{a_L b_L c_L}}$ represents the scale factor. Both $\log\frac{a_L}{\sqrt[3]{a_L b_L c_L}}$ and $\log\frac{R_L(p)}{\sqrt[3]{R_L(p)G_L(p)B_L(p)}}$ are redefined as α_L and K_L, respectively. The new formula of Eq. 5 is shown as Eq. 6.

$$R''_L(p) = \alpha_L + \gamma_L K_L(p) \tag{6}$$

To eliminate the scale factor α_L, a bilateral filter is used [8]. This filter is based on a patch. Eq. 7 shows the process of eliminating the scale factor using the bilateral filter.

$$R'''_L(t) = R''_L(t) - \frac{\sum_{t\in W(p)} w(t) R''_L(t)}{Z(p)} \tag{7}$$

where $R'''_L(t)$ represents the color value from which the scale factor is removed, t is an element of the set of pixels $W(p)$ in the patch whose center pixel is p, w is a weighting function of the bilateral filter, and Z is a sum of weighting values in the patch.

The bilateral filter is applied to all R''_L values in the patch. Subsequently, each filtered value is subtracted from R''_L. As a result, the scale factor is eliminated. Eq. 7 is rearranged to obtain Eq. 8.

$$R'''_L(t) = \gamma_L \left(K_L(t) - \frac{\sum_{t\in W(p)} w(t) K_L(t)}{Z(p)} \right) \tag{8}$$

The gamma exponent can be ignored in the process of similarity measure using an equation of the normalized cross correlation (NCC). The ANCC of R channel is defined in Eq. 9.

$$ANCC_R(f_p) = \frac{\sum_{i=1}^{M} w_L(t_i) w_R(t_i) [R'''_L(t_i)] \times [R'''_R(t_i)]}{\sqrt{\sum_{i=1}^{M} |w_L(t_i) R'''_L(t_i)|^2} \times \sqrt{\sum_{i=1}^{M} |w_R(t_i) R'''_R(t_i)|^2}} \tag{9}$$

where $ANCC_R$ is the ANCC value of R channel when the disparity value is f_p, f_p indicates the disparity candidate of pixel p, both w_L and w_R are bilateral weighting functions for patches in the left and the right images, respectively, and M represents the patch size. The $M \times M$ sized patch centered at p is used for the ANCC. The NCC equation is applied to each pixel t_i in the patch. $ANCC_G$ and $ANCC_B$ can be obtained in the same way as previously described.

As a result, the cost function of the ANCC is defined in Eq. 10, where $D(f_p)$ is the matching cost using the ANCC.

$$D(f_p) = 1 - \frac{ANCC_R(f_p) + ANCC_G(f_p) + ANCC_B(f_p)}{3} \tag{10}$$

The similarity measure using the ANCC method enhances the disparity search under the radiometric variation. Fig. 1 shows stereo matching results under the radiometric variation. Fig. 1(a) is an original left viewpoint image, Fig. 1(b) is a matching result using the intensity and the gradient values for the cost computation [3], and Fig. 1(c) is the result using the ANCC.

In Fig. 1(b), there are significant errors because of the radiometric change. On the other hand, Fig. 1(c) shows a better quality disparity map than Fig. 1(b).

The ANCC is robust to radiometric changes. However, it requires significant cost computation time to execute because the bilateral filter requires high computational complexity. In addition,

the ANCC also performs patch-based matching. Therefore, the larger the patch size, the higher the complexity of the computation. For this reason, the ANCC is not suitable for real-time stereo matching under different radiometric conditions.

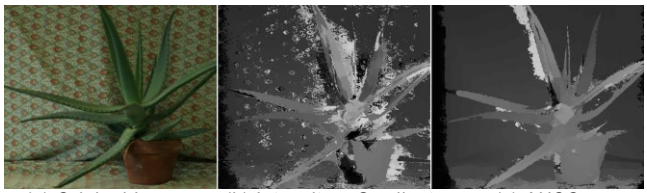

(a) Original Image (b) Intensity + Gradient (c) ANCC

Figure 1. Stereo Matching Results Under Radiometric Change

3. Pixel-Based ANCC Cost Computation

3.1 Scale Factor Removal with Global Mean Value

The conventional ANCC uses the bilateral filter to remove the scale factor α_L in Eq. 6. The bilateral filter is applied to every pixel in the image for the scale factor removal. This filtering process has the advantage of eliminating the scale factor while preserving the edge region. However, it takes a lot of time. To reduce the time for scale factor removal, a global mean value is used [5, 6].

The global mean value indicates the average color value of all pixels in the image. This value is not computed repeatedly, like the bilateral filtering process, but requires only one computation for each channel. An equation of the global mean is defined as follows

$$M_R(p) = \frac{\sum_{t \in W_{MN}} R_L''(t)}{MN} \tag{11}$$

where $M_R(p)$ means the global mean value of R_L'' at centered pixel p, t is a pixel in the image W_{MN}, M and N are a width and a height of W_{MN}, respectively.

M_G and M_B for G_L'' and B_L'' are calculated in the same manner. Eq. 11 is applied to Eq. 7 instead of the bilateral filtering process. Therefore, Eq. 7 is redefined in Eq. 12.

$$R_L'''(p) = R_L''(p) - M_R(p) \tag{12}$$

In Eq. 12, $R_L''(p)$ is equal to $\alpha_L + \gamma_L K_L(p)$. Thus, the scale factor α_L is eliminated by $M_R(p)$ as depicted in Eq. 13.

$$R_L'''(p) = \gamma_L \left(K_L(p) - \frac{\sum_{t \in W_{MN}} K_L(t)}{MN} \right) \tag{13}$$

3.2 Gamma Exponent Removal with Hue Transform

The global mean value eliminates the scale factor quickly and easily. However, the gamma exponent still remains in Eq. 13. To remove the gamma exponent, the conventional ANCC uses the equation of the NCC. The NCC equation offsets the gamma exponents of the numerator and the denominator in Eq. 9. The objective of the proposed method is the pixel-based cost computation for the illumination invariant stereo matching. Using patch-based matching, the proposed method removes the gamma exponent using an equation of hue transform [9].

Hue is one of the three elements of the HSI model [9]. This model shows how color objects viewed by humans are analyzed. The HSI model includes hue, saturation, and intensity. The RGB color model can be transformed to the HSI model by using several equations. Eq. 14, Eq. 15, and Eq. 16 are the hue transform, the saturation transform, and the intensity transform, respectively.

$$\theta = \cos^{-1}\left\{ \frac{\frac{1}{2}[(R-G)(R-B)]}{[(R-G)^2 + (R-B)(G-B)]^{1/2}} \right\} \tag{14}$$

$$S = 1 - \frac{3}{(R+G+B)}[\min(R,G,B)] \tag{15}$$

$$I = \frac{1}{3}(R+G+B) \tag{16}$$

The hue transform in Eq. 14 is independent of the scale value. If the gamma value in Eq. 13 is a scale value, that value can be eliminated by replacing R_L''', G_L''', and B_L''' instead of R, G, and B, respectively, in Eq. 14. Assuming that $K_L(p) - \frac{\sum_{t \in W_{MN}} K_L(t)}{MN}$ is equal to T_R, $R_L'''(p)$ is the same with $\gamma_L T_R$. Similarly, $G_L'''(p)$ and $B_L'''(p)$ can be defined as $\gamma_L T_G$ and $\gamma_L T_B$, respectively. Therefore, R_L''', G_L''', and B_L''' values are defined as one hue value whose gamma value is removed by the hue transformation. The hue value from which the gamma value is removed is defined as follows.

$$\theta = \cos^{-1}\left\{ \frac{\frac{1}{2}[(T_R - T_G)(T_R - T_B)]}{[(T_R - T_G)^2 + (T_R - T_B)(T_G - T_B)]^{1/2}} \right\} \tag{17}$$

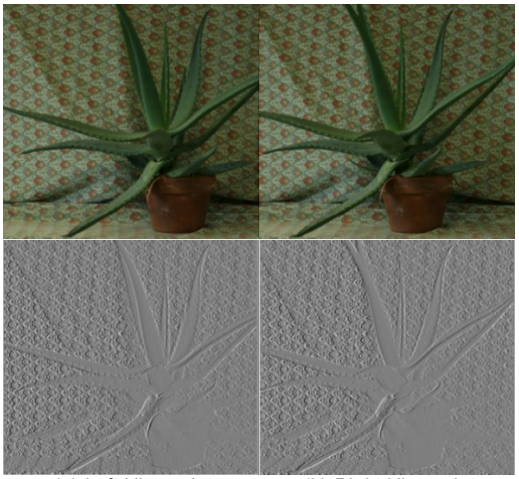

(a) Left Viewpoint (b) Right Viewpoint

Figure 2. Gradient Images

The final cost function $C(f_p)$ includes the gradient and the hue values. It is defined in Eq. 18.

$$C(f_p) = \alpha \cdot \nabla_x I(f_p) + (1-\alpha) \cdot \theta(f_p) \quad (18)$$

In Eq. 18, $\theta(f_p)$ is the hue value of the pixel which is distant from the current pixel p by the disparity value f_p. $\nabla_x I$ is the matching cost between gradient images. It is calculated by the pixel-based measure. To calculate this matching cost, two color images should be changed to gradient images as depicted in Fig. 2.

In Fig. 2, the first row represents the original color images and the second row shows the gradient images. The weighting value α adjusts the balance between $\theta(f_p)$ and $\nabla_x I(f_p)$. It is a constant value specified by the user. To aggregate the matching cost, the cross-scale cost aggregation method was used [2].

4. Experiment Results

4.1 Weighting Value Decision

Four stereo images were used for the experiment: *Aloe, Art, Moebius, and Dolls.* Each image is tested under twelve different radiometric conditions. Six of the twelve kinds of radiometric changes are controlled by exposure and the remaining six are controlled by illumination. To determine the weighting value in Eq. 18, we compared the error rates according to the weighting values from 0 to 1. The graph of the error rate change according to the weighting value is depicted in Fig. 4.

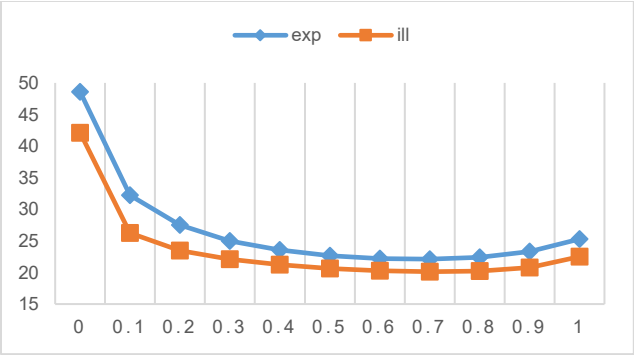

Figure 3. Error Rate Change

In Fig. 3, the *x*-axis represents the weighting value α and the *y*-axis means the error rate. the error rate is represented as the percentage. The diamond points represent the error rates under exposure changes. The square points mean the error rates under illumination changes. Depending on the results of Fig. 3, the weighing value α was set to 0.7 for the experiment.

4.2 Error Rate and Cost Computation Time

For the objective performance evaluation, we used the bad pixel rate as the error rate comparison standard. We measured error rates in non-occluded regions. Table 1 shows error rates under exposure changes.

In Table 1, the first column shows test images and their conditions. There are two numbers next to the image name for each test image. The left side number indicates the exposure level of the left viewpoint image and the right side number indicates that of the right viewpoint image. The exposure level ranges from 0 to 2. The intensity + gradient method uses intensity and gradient values for the similarity measure [3]. The MANCC method is our another method that was published in other conference [5, 6]. This method uses the census transform instead of the hue transform to remove the gamma exponent. The average error rate obtained in the non-occluded region is the smallest for our method when compared to other conventional methods.

Table 1: Error Rates under Exposure Changes

	Intensity + gradient [3]	ANCC [4]	MANCC [5, 6]	Our method
Aloe(0_0)	12.74	21.03	20.43	13.44
Aloe(0_1)	34.55	22.15	35.12	28.53
Aloe(0_2)	42.4	21.72	33.37	33.77
Aloe(1_1)	10.43	14.03	14.63	12.24
Aloe(1_2)	19.77	13.82	14.83	15.65
Aloe(2_2)	9.85	11.73	12.47	11.93
Art(0_0)	15.05	33.8	32.74	18.46
Art(0_1)	42.78	34.92	43.25	36.20
Art(0_2)	54.05	38.95	43.06	46.17
Art(1_1)	12.82	21.41	19.62	15.88
Art(1_2)	28.43	23.91	24.86	26.21
Art(2_2)	14.84	20.79	19.41	18.3
Moebius(0_0)	14.8	25.37	24.68	15.35
Moebius(0_1)	33.42	24.85	23.55	22.17
Moebius(0_2)	39.13	29.15	24.81	27.70
Moebius(1_1)	11.69	17.26	16.86	13.02
Moebius(1_2)	20.54	22.12	18.31	18.08
Moebius(2_2)	13.98	16.72	16.75	15.79
Dolls(0_0)	11.71	25.13	24.69	13.19
Dolls(0_1)	39.47	31	43.33	35.93
Dolls(0_2)	46.83	32.83	45.86	44.31
Dolls(1_1)	8.85	16.93	16.49	11.16
Dolls(1_2)	30.16	20.09	18.55	24.94
Dolls(2_2)	9.4	12.73	12.09	12.26
Avg.	24.07	23.02	24.99	22.11

Table 2 represents error rates under illumination changes. Unlike the exposure level, the illumination level ranges from 1 to 3. In Table 2, all error rates were measured in non-occluded regions. The average error rate of the MANCC has the smallest value among implemented algorithms, including our method. However, our method performed better than the intensity + gradient method.

Error rates are graphically illustrated in Figs. 4 and 5 to make it easier to analyze error rate variations caused by radiometric changes. Fig. 4 shows the error graph for exposure changes and Fig. 5 represents the error graph for illumination changes. Both figures represent the average error rates of all test images for each radiometric condition.

In Fig. 4, the conventional ANCC shows the most stable performance under radiometric changes. In Fig. 5, both the conventional ANCC and the MANCC have more stable error rate variation than that of the proposed method. However, our method a better performance than that of the intensity + gradient method.

Table 2: Error Rates under Illumination Changes

	Intensity + gradient [3]	ANCC [4]	MANCC [5, 6]	Our method
Aloe(1_1)	10.43	14.03	14.63	12.24
Aloe(1_2)	17.69	17.35	28.7	16.49
Aloe(1_3)	33.34	18.98	26.82	24.50
Aloe(2_2)	10.05	13.73	14.84	11.39
Aloe(2_3)	24.83	18.84	20.94	20.09
Aloe(3_3)	10.1	14.9	15.52	11.10
Art(1_1)	12.82	21.41	19.62	15.88
Art(1_2)	21.7	23.27	20.53	20.67
Art(1_3)	43.4	35.92	32.66	41.16
Art(2_2)	12.75	20.74	19.22	16.07
Art(2_3)	37.85	30.05	27.97	37.07
Art(3_3)	13.12	20.79	18.74	16.25
Moebius(1_1)	11.69	17.26	16.86	13.02
Moebius(1_2)	17.28	18.06	16.26	16.23
Moebius(1_3)	32.83	22.24	20.1	28.03
Moebius(2_2)	12.64	18.23	16.92	14.17
Moebius(2_3)	25.8	20.28	18.54	23.09
Moebius(3_3)	12.61	17.3	15.71	13.29
Dolls(1_1)	8.85	16.93	16.49	11.16
Dolls(1_2)	20.66	18.81	16.67	18.78
Dolls(1_3)	53	28.99	28.17	46.45
Dolls(2_2)	8.7	16.13	15.09	11.03
Dolls(2_3)	37.65	22.66	21.11	33.31
Dolls(3_3)	9.21	15.39	14.13	11.50
Avg.	20.79	20.1	19.84	20.12

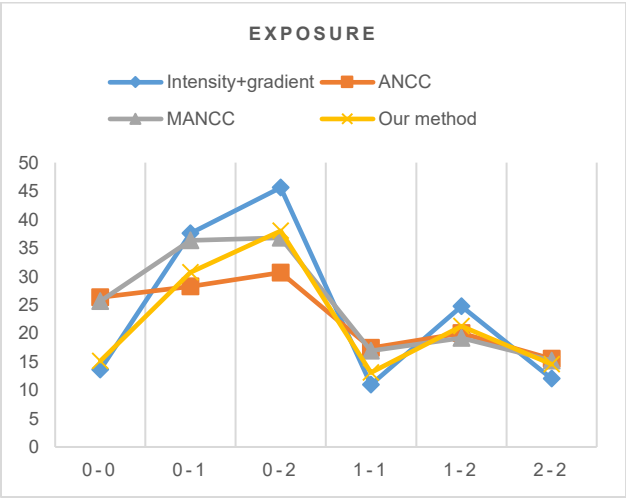

Figure 4. Error Rate Graph for Exposure Changes

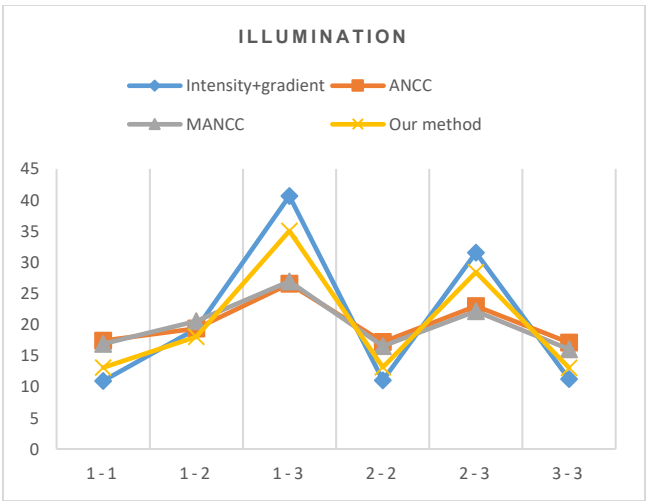

Figure 5. Error Rate Graph for Illumination Changes

Table 3: Cost Computation Time Comparison

Algorithm	Time (sec.)
Intensity + gradient [3]	0.4
ANCC [4]	116.93
MANCC [5, 6]	39.07
Proposed method	0.4

Table 3 represents the time required to compute the cost. As a result, we can confirm that the proposed method is faster than the conventional ANCC and the MANCC. The resulting images are shown in Fig. 6. In Fig. 6, the results of *Aloe*, *Art*, *Moebius*, and *Dolls* are displayed in order from top to bottom. Those are the matching results between illumination level 1 and level 3.

5. Conclusion

The stereo matching method under varying radiometric factors causes disparity errors in the resulting disparity map. The ANCC is one of the measures for the illumination invariant stereo matching. It performs well under various exposure and illumination conditions. However, it incurs significant cost computation time because of the bilateral filtering process and the patch-based measure. To reduce the cost computation time, we proposed the pixel-based ANCC. The proposed method uses the global mean value instead of the bilateral filter to remove the scale factor. Additionally, it also uses the hue transform to remove the gamma value. The performance of the proposed method was slightly worse than that of the conventional ANCC method, but the cost computation time was faster than that of the ANCC.

Acknowledgement

This work was supported in part by the National Research Foundation of Korea(NRF) Grant funded by the Korean Government(MSIP)(No. 2011-0030079), and in part by the 'Brain Korea 21 Plus Project' of the Ministry of Education & Human Resources Development, Republic of Korea (ROK) [F16SN26T2205].

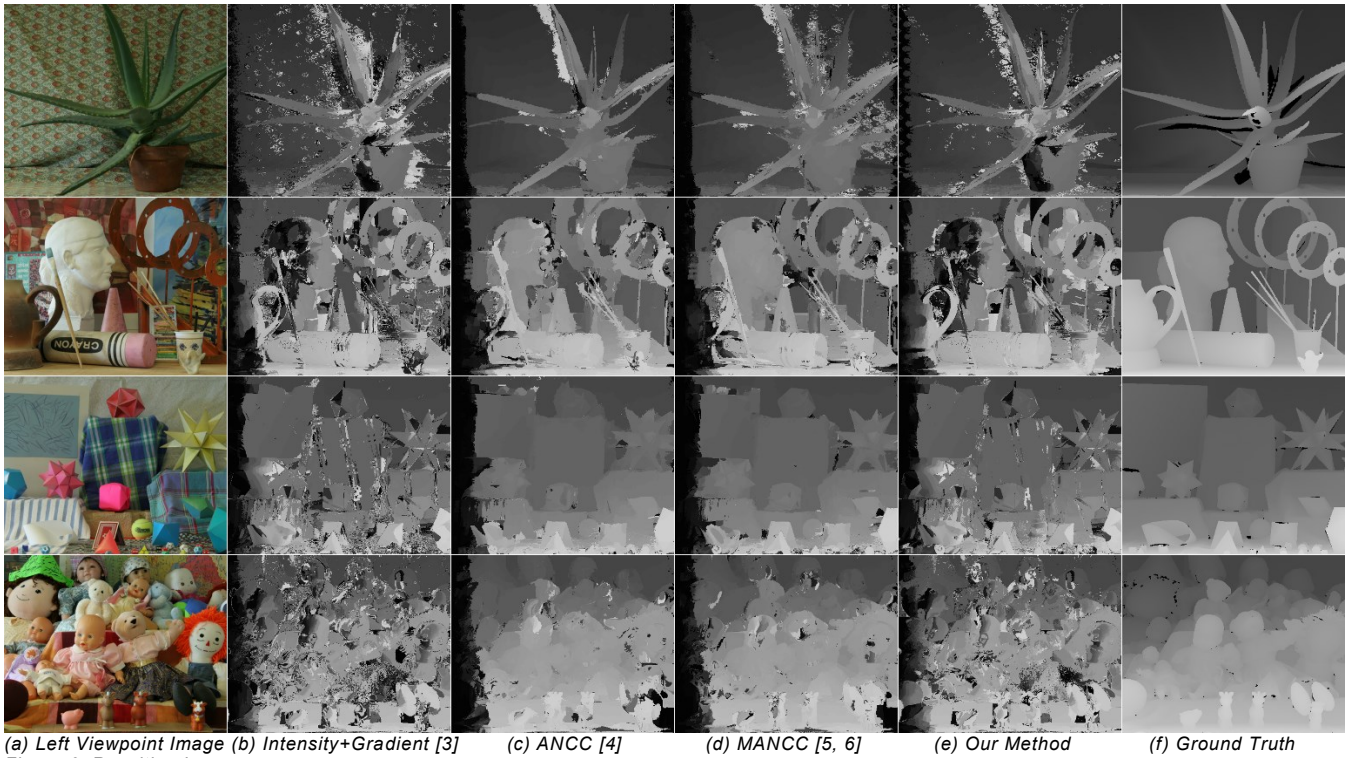

(a) Left Viewpoint Image (b) Intensity+Gradient [3] (c) ANCC [4] (d) MANCC [5, 6] (e) Our Method (f) Ground Truth

Figure 6. Resulting Images

References

[1] Y. S. Kang and Y. S. Ho, "An efficient image rectification method for parallel multi camera arrangement," IEEE Transactions on Consumer Electronics, vol. 57, issue 3, pp. 1041-1048, Aug. 2011.

[2] K. Zheng, Y. Fang, D. Min, L. Sun, S. Yang, S. Yan, and Q. Tian, "Cross-scale cost aggregation for stereo matching," IEEE Conference on Computer Vision and Pattern Recognition, pp. 1590-1597, June 2014.

[3] C. Rhemann, A. Hosni, M. Bleyer, C. Rother, and M. Gelautz, "Fast cost-volume filtering for visual correspondence and beyond," IEEE Conference on Computer Vision and Pattern Recognition, pp. 3017-3028, June 2011.

[4] Y. S. Heo, K. M. Lee, and S. U. Lee, "Illumination and camera invariant stereo matching," IEEE Conference on Computer Vision and Pattern Recognition, pp. 1-8, Aug. 2008.

[5] Y. J. Chang and Y. S. Ho, "Robust stereo matching to radiometric variation using binary information of census transformation," Korean Institute of Broadcast and Media Engineers Fall Conference, pp. 1-2, Nov. 2016.

[6] Y. J. Chang and Y. S. Ho, "Fast cost computation using binary information for illumination invariant stereo matching," IEEE Seoul Section Student Paper Contest, pp. 1-4, Dec. 2016.

[7] G. D. Finlayson and S. D. Hordley, "Illuminant and gamma comprehensive normalization in log RGB space," Pattern Recognition Letters, vol. 24, no. 11, pp. 1679-1690, July 2003.

[8] C. Tomasi and R. Manduchi, "Bilateral filtering for gray and color images," IEEE Sixth International Conference on Computer Vision, pp. 839-846, Jan. 1998.

[9] R. C. Gonzalez and R. E. Woods, "Digital image processing, third ed.," Pearson Education, pp. 429-436, 2010.

Author Biography

Yong-Jun Chang received his B.S. in electronic engineering and avionics from the Korea Aerospace University, Gyeonggi-do, Korea (2014) and his M.S. in electrical engineering and computer science from the Gwangju institute of Science and Technology, Gwangju, Korea (2016). Since then he has studied in the Gwangju Institute of Science and Technology in Gwangju, Korea for Ph.D. courses. His research interests are stereo matching, video coding, and image processing.

Yo-Sung Ho received his B.S. and M.S. degrees in electronic engineering from Seoul National University, Seoul, Korea (1981, 1983) and his Ph.D. in electrical and computer engineering from University of California, Santa Barbara, USA (1990). He worked at ETRI from 1983 to 1995, and Philips Laboratories from 1990 to 1993. Since 1995, he has been with Gwangju Institute of Science and Technology, Gwangju, Korea, where he is currently a professor. His research interests include video coding, 3D image processing, 3DTV, AR/VR, and realistic broadcasting systems.